

## ADIABATIC HEATING AND CONVECTION IN A POROUS MEDIUM FILLED WITH A NEAR-CRITICAL FLUID

**E. B. Soboleva**  
 Institute for Problems in Mechanics RAS, Moscow

### ABSTRACT

Dynamics and heat transfer in a porous medium filled with a fluid phase at parameters near the gas-liquid critical point are studied. A two-dimensional numerical solver based on the hydrodynamic model for a porous medium with a high compressible fluid phase including the van der Waals equation of state is used. In weightlessness, adiabatic heating of fluid phase under the step-temperature heat supply is investigated analytically and numerically. In terrestrial conditions, gravity-driven convection in vertical rectangular cells generated by lateral heating in unsteady and steady-state regimes is simulated. The effects of high compressibility of near-critical fluid phase on convection are studied. Convective motions and heat transfer in horizontal rectangular cells consisting of two porous layers at different porosity and permeability heated from below are simulated as well. Adiabatic heating subjected to hydrostatic compressibility effects, the onset and development of convection, and convective structures in a steady-state regime are analysed.

### NOMENCLATURE

$t$	time	$T$	temperature
$\tau_{pe}$	characteristic time of the piston effect	$\varepsilon$	reduced temperature, $\varepsilon = (T - T_c) / T_c$
$\tau_d$	characteristic time of thermal diffusion	$s$	entropy (per mass)
$x, y$	position coordinates	$S$	entropy (per volume)
$l$	length	$\sigma$	ratio of heat capacities, $\sigma = \rho_m' c_m' / \rho_c' c_{v0}'$
$h$	height	$\lambda$	thermal conductivity
$\bar{g}$	mass force acceleration	$\beta$	thermal expansion coefficient
$\rho$	density	$D$	thermal diffusivity
$\bar{V}$	fluid velocity	$c$	heat capacity
$\bar{U}$	filtration velocity, $\bar{U} = (u, v)$	$c_v$	heat capacity of fluid at constant volume
$P$	total pressure	$c_p$	heat capacity of fluid at constant pressure
$\langle P \rangle$	volume-average pressure	$\eta$	viscosity
$p$	dynamic pressure	$\varphi$	porosity
		$K$	permeability
		$d\varpi$	elementary volume
		$\Omega$	full volume
		$ds$	elementary surface
		$B$	constant, $B = R / \mu_g$
		$R$	universal gas constant, $R = 8,31 \text{ J}/(\text{K}\cdot\text{mol})$
		$\mu_g$	molecular weight
		$Nu$	Nusselt number
		$Re$	Reynolds number
		$Da$	Darcy number
		$M$	Mach number
		$\Theta$	characteristic temperature difference at boundaries
		$\gamma_0$	ratio of specific heats
		$Ra_{d0}$	model Rayleigh-Darcy number
		$Ra_d$	real Rayleigh-Darcy number
		$Pr_0$	model Prandtl number
		$Pr$	real Prandtl number

## Subscripts

$f$	fluid phase
$s$	solid phase
$m$	porous medium
$c$	critical value
$i$	initial value
0	reference value (far from critical)

## Superscripts

'	dimensional value
---	-------------------

## 1. INTRODUCTION

Substances at parameters near the gas-liquid critical point known as near-critical fluids are of great interest due to specific thermodynamic and transport properties leading to strong thermo-mechanical coupling and significant peculiarities in their dynamic behavior. With approach to the critical point, the specific heat at constant pressure and the compressibility grow unboundedly whereas the thermal diffusivity goes to zero<sup>1</sup>. Dynamics and heat transport in single-phase near-critical fluids were investigated extensively both in microgravity conditions in orbital flies (see Refs. 2-6 and references cited therein) and on Earth in laboratory experiments<sup>7,8</sup>. A seemingly puzzling observation in space<sup>9</sup> stimulated a theoretical analysis<sup>10,11</sup> which has revealed that adiabatic heating called the piston effect is the dominant temperature equilibration mechanism near criticality. Numerical simulations by different groups confirmed this prediction and gave many new results on features of the piston effect in different conditions, an interplay between convection and the piston effect, instability problems, and an influence of gravity force on complicated dynamics and heat transport near the critical point (see Refs. 12-18 and references cited therein).

However, the problems of near-critical dynamics inside porous media are poorly understood despite their different applications in geophysics and energy-related systems. Only several numerical researches<sup>19,20</sup> in this field associated with convection were carried out. The obtained results drew simplified dynamic and thermal patterns since a near-critical phase was modeled in the Oberbeck-Boussinesq approximation excluding effects of adiabatic heating. Recently, an asymptotic analysis of complex one-dimensional hydrodynamic equations of high compressible van der Waals fluid in a porous medium was performed<sup>21</sup> showing some peculiarities of the piston effect inside a porous matrix.

In this paper, a mathematical model based on hydrodynamic equations of porous media and the van der Waals equation of state of fluid phase is developed. The model describes effects governed by abnormal thermodynamic and transport coefficients, hydrostatic compressibility effects, adiabatic heating, and effects of solid matrix. Based on this model, a novel two-dimensional semi-implicit numerical code was designed. In weightlessness, the piston effect in a porous

layer stimulated by step-temperature heating is studied analytically and numerically. The expression of the characteristic time of the piston effect is found. The obtained results are compared with the known solution for a single-phase near-critical fluid. In gravity field, convection in vertical and two-layer horizontal cells under side and bottom heating in unsteady and steady-state regimes is simulated. The correlation relations are derived and a comparison with dynamics of ideal gas is carried out. An influence of adiabatic heating on convection and hydrostatic effects on adiabatic heating, the onset and development of convection, stated convective structures and effects of solid matrix are analyzed.

## 2. MATHEMATICAL MODEL

To derive the energy equation of an isotropic porous medium, first, the energy equations of solid and fluid phases are written separately. In dimensional form, these equations are as follows:

$$(1 - \varphi)\rho_s'c_s'\frac{\partial T_s'}{\partial t'} = (1 - \varphi)\nabla(\lambda_s'\nabla T_s') + q_v' \quad (2.1)$$

$$\begin{aligned} \varphi\rho_f'c_v'\frac{\partial T_f'}{\partial t'} + \varphi\rho_f'c_v'(\bar{\mathbf{V}}_f'\nabla)T_f' = \\ = -\varphi T_f'\left(\frac{\partial P'}{\partial T_f'}\right)_{\rho'}\nabla\bar{\mathbf{V}}_f' + \varphi\nabla(\lambda_f'\nabla T_f') - q_v' \end{aligned} \quad (2.2)$$

The equation of fluid phase is multiplied by the porosity  $\varphi$  and that of solid phase by the factor  $(1 - \varphi)$  to give the balance relations in an elementary unit volume. The term  $q_v'$  in Eqs. (2.1) and (2.2) describes the interphase heat exchange. Further we assume that there is local thermal equilibrium so that the temperatures of solid and fluid phases are equal to each other, i.e.  $T_s' = T_f' = T'$ . Adding Eqs. (2.1) and (2.2), and replacing fluid velocity  $\bar{\mathbf{V}}_f'$  by the filtration velocity  $\bar{\mathbf{U}}' = \varphi\bar{\mathbf{V}}_f'$ , we lead to the energy equation in the form:

$$\begin{aligned} \rho_m'c_m'\frac{\partial T'}{\partial t'} + \rho_f'c_v'(\bar{\mathbf{U}}'\nabla)T' = \\ = -T'\left(\frac{\partial P'}{\partial T'}\right)_{\rho'}\nabla\bar{\mathbf{U}}' + \nabla(\lambda_m'\nabla T') \end{aligned} \quad (2.3)$$

Here, the variables  $\rho_m'c_m'$  and  $\lambda_m'$  are associated with a porous medium as a whole:

$$\rho_m'c_m' = (1 - \varphi)\rho_s'c_s' + \varphi\rho_f'c_v' \quad (2.4)$$

$$\lambda_m' = (1 - \varphi)\lambda_s' + \varphi\lambda_f' \quad (2.5)$$

The energy equation of porous medium Eq. (2.3) includes the work done by pressure in a fluid phase which is described by the first term in the right-hand side. This term allows us to simulate effects of adiabatic heating that is impossible in the classical model based on Oberbeck-Boussinesq approximation.

One can derive the energy equation in another form. We start with the energy equation of fluid phase written as

$$\begin{aligned} \varphi \rho_f' c_p' \frac{\partial T_f'}{\partial t'} + \varphi \rho_f' c_p' (\bar{\mathbf{V}}_f' \nabla) T_f' = \\ = -\varphi \frac{T_f'}{\rho_f'} \left( \frac{\partial \rho_f'}{\partial T_f'} \right)_{P'} \frac{dP'}{dt'} + \varphi \nabla (\lambda_f' \nabla T_f') - q_v' \end{aligned} \quad (2.6)$$

Equation (2.6) may be transformed into Eq. (2.2) using the relation  $P' = P'(\rho_f', T_f')$  and the continuity equation. Adding Eqs. (2.1) and (2.6) with the assumption of local thermal equilibrium, we obtain the energy equation of porous medium in the form:

$$\begin{aligned} \rho_m' c_m^P \frac{\partial T'}{\partial t'} + \varphi \rho_f' c_p' (\bar{\mathbf{U}} \nabla) T' = \\ = -\varphi \frac{T'}{\rho_f'} \left( \frac{\partial \rho_f'}{\partial T'} \right)_{P'} \frac{dP'}{dt'} + \nabla (\lambda_m' \nabla T') \end{aligned} \quad (2.7)$$

In Eq. (2.7), the conductivity  $\lambda_m'$  is defined by the relation (2.5). The variable  $\rho_m' c_m^P$  includes the heat capacity at constant pressure and is defined as

$$\rho_m' c_m^P = (1 - \varphi) \rho_s' c_s' + \varphi \rho_f' c_p' \quad (2.8)$$

Equations (2.3) and (2.7) are the equal to each other. It is convenient to include Eq. (2.3) to the mathematical model below but to use Eq. (2.7) in the analysis of the piston effect in the next section.

A mathematical model consists of the ordinary continuity and momentum equations for an isotropic porous medium with a compressible fluid phase<sup>22</sup>, the energy equation in the form of Eq. (2.3), and the van der Waals equation of state. The pressure  $P'$  is decomposed into two components (a volume-average part  $\langle P' \rangle$  and a rest part  $p'$  associated with dynamic changes) so that  $P' = \langle P' \rangle + p'$ . The part  $\langle P' \rangle$  is independent of space variables, therefore the gradient  $\nabla P'$  in the momentum equation may be replaced by the gradient  $\nabla p'$ . To

close the set of equations, the relation  $\frac{1}{\Omega'} \int_{\Omega'} p' d\varpi' = 0$

resulted from the condition on the term  $\langle P' \rangle$  to be the average value is included.

The government equations are transformed into dimensionless form. The scales are: length  $l'$ , velocity  $U'$ , time  $l'/U'$ , mass force acceleration  $g'$ , critical parameters  $\rho_c'$  and  $T_c'$ , coefficients  $\eta_0'$ ,  $c_{v0}'$ ,  $K_0'$ ,  $\lambda_{m0}'$  (thermal conductivity  $\lambda_{m0}'$  is defined as  $\lambda_{m0}' = (1 - \varphi) \lambda_s' + \varphi \lambda_{f0}'$ ), pressure  $B' \rho_c' T_c'$  for  $P'$  and  $\langle P' \rangle$  whereas  $\rho_c' U'^2$  for  $p'$ . For the simplicity, the density of fluid  $\rho_f'$  loses the subscript  $f$ . The government equations are:

$$\varphi \frac{\partial \rho}{\partial t} + \nabla (\rho \bar{\mathbf{U}}) = 0 \quad (2.9)$$

$$\frac{\rho}{\varphi} \frac{\partial \bar{\mathbf{U}}}{\partial t} = -\nabla p + \frac{Ra_{d0}}{\Theta Re^2 Da Pr_0} \rho \bar{\mathbf{g}} - \frac{1}{Da Re K} \bar{\mathbf{U}} \quad (2.10)$$

$$\begin{aligned} \rho_m c_m \frac{\partial T}{\partial t} + \rho (\bar{\mathbf{U}} \nabla) T = \\ = -(\gamma_0 - 1) \frac{\rho T}{1 - \rho/3} \nabla \bar{\mathbf{U}} + \frac{\gamma_0}{Re Pr_0} \nabla (\lambda_m \nabla T) \end{aligned} \quad (2.11)$$

$$\rho_m c_m = (1 - \varphi) \rho_s c_s + \varphi \rho, \quad \lambda_m = 1 + \varphi (\lambda_f - \lambda_0) \quad (2.12)$$

$$P = \frac{\rho T}{1 - \rho/3} - 9/8 \rho^2 \quad (2.13)$$

$$P = \langle P \rangle + \gamma_0 M^2 p, \quad \int_{\Omega} p d\varpi = 0 \quad (2.14)$$

Dimensionless values are without primes. The dimensionless parameters are

$$\begin{aligned} Ra_{d0} = \frac{\Theta' g' l' K_0' \rho_c'^2 (c_{v0}' + B')}{T_c' \lambda_{m0}' \eta_0'}, \quad Re = \frac{\rho_c' U' l'}{\eta_0'} \\ Da = \frac{K_0'}{l'^2}, \quad Pr_0 = \frac{(c_{v0}' + B') \eta_0'}{\lambda_{m0}'}, \quad M = \frac{U'}{\sqrt{\gamma_0 B' T_c'}} \\ \Theta = \frac{\Theta'}{T_c'}, \quad \gamma_0 = 1 + \frac{B'}{c_{v0}'} \end{aligned} \quad (2.15)$$

Initially, the temperature is uniform, and the velocity is zero. The fluid phase is stratified according to the linear relations:

$$\rho = \rho^+ \left( 1 + \left( \frac{(3-\rho)^2}{9T - \frac{9\rho}{4}(3-\rho)^2} \right) \frac{\gamma_0 M^2}{Fr} \bar{\mathbf{g}}(\bar{\mathbf{r}} - \bar{\mathbf{r}}^+) \right)$$

$$p = p^+ + \rho^+ \frac{1}{Fr} \bar{\mathbf{g}}(\bar{\mathbf{r}} - \bar{\mathbf{r}}^+), \quad \frac{1}{Fr} = \frac{Ra_{d0}}{\Theta Re^2 Da Pr_0} \quad (2.16)$$

The subscript «+» marks values in the center of volume. The fluid slips at boundaries.

The thermal conductivity increases with approach to the critical point according to a power-law relation. In a pure near-critical fluid, we use the relation<sup>6,14-18</sup>  $\lambda_f' = \lambda_0'(1 + \Lambda((T' - T_c')/T_c')^{-\psi})$  which leads to the dimensionless relation in a porous medium:  $\lambda_m = 1 + \varphi \lambda_0 \Lambda(T - 1)^{-\psi}$ .

The novel 2D numerical solver based on a finite-difference formulation has been designed. The space discretization on a straggled grid using second-order implicit schemes is employed. Nonuniform rectangular grids are used. The equations are integrated successively. The momentum equation is solved by SIMPLE-type algorithm<sup>23</sup>. As mentioned above, two-scale splitting of the pressure in the government equations was carried out. This procedure has allowed us to design an effective numerical code for simulations of low-speed dynamic phenomena at a large time step. In the limit of small Mach numbers the model applied approaches to the acoustic-filtering model<sup>24</sup>. However, we do not exclude sonic waves and may simulate acoustic processes as well.

### 3. PISTON EFFECT

#### 3.1. THEORETICAL ANALISYS

An analysis of the piston effect in a porous layer is performed in a fashion analogous to that in a single-phase fluid based on a linear thermodynamic approach<sup>13</sup>.

A porous cell of fixed volume  $\Omega'$  containing a near-critical fluid is considered. The initial temperature of system is constant. The temperature at one boundary rises initiating thermal processes inside the cell. Body forces are equal to zero.

We consider the entropy per mass  $s_m'$ . The entropy variation  $\delta s_m'$  may be expressed by the density and pressure variations  $\delta \rho_m'$  and  $\delta P'$  as

$$\delta s_m' = \left( \frac{\partial s_m'}{\partial \rho_m'} \right)_{P'} \delta \rho_m' + \left( \frac{\partial s_m'}{\partial P'} \right)_{\rho_m'} \delta P' \quad (3.1)$$

Equation (3.1) is averaged in the space to result in the expression of the average variation entropy

$\langle s_m' \rangle = \frac{1}{\Omega'} \int \delta s_m' d\varpi'$ . Since the volume of cell is constant, the term of density variation is vanishing:  $\frac{1}{\Omega'} \int \left( \frac{\partial s_m'}{\partial \rho_m'} \right)_{P'} \delta \rho_m' d\varpi' = 0$ . The pressure variation is assumed to be uniform in space. We obtain

$$\langle s_m' \rangle = \left( \frac{\partial s_m'}{\partial P'} \right)_{\rho_m'} \delta P' \quad (3.2)$$

The process is in equilibrium and the entropy variation  $\delta S_m'$  (per volume) is determined by the heat supply  $\delta q'$ :  $T' \delta S_m' = \delta q'$ . Integrating the last equation in the space and using the relation:  $S_m' = \rho_m' s_m'$ , we have

$$\frac{1}{\Omega'} \int T' \delta(\rho_m' s_m') d\varpi' = \frac{1}{\Omega'} Q' \quad (3.3)$$

where  $Q'$  is the net heat amount. The left-hand side of Eq. (3.3) may be transformed with the use of the average variation entropy giving

$$T' \rho_m' \langle \delta s_m' \rangle = \frac{1}{\Omega'} Q' \quad (3.4)$$

From Eqs. (3.2) and (3.4), one can obtain

$$\delta P' = \left( \frac{\partial P'}{\partial s_m'} \right)_{\rho_m'} \frac{1}{T' \rho_m' \Omega'} Q' \quad (3.5)$$

Further, the energy equation in the form of Eq. (2.7) is considered. Going, in the left-hang side, from the partial time derivative to the total derivative, we find

$$\begin{aligned} \rho_m' c_m^p \frac{dT'}{dt} - (1-\varphi) \rho_s' c_s' (\bar{\mathbf{U}}' \cdot \nabla) T' = \\ = -\varphi \frac{T'}{\rho_f'} \left( \frac{\partial \rho_f'}{\partial T'} \right)_{P'} \frac{dP'}{dt} + \nabla(\lambda_m' \nabla T') \end{aligned} \quad (3.6)$$

Equation (3.6) is applied to the interior (bulk) region of cell beyond the thermal boundary layer. In this region, the thermal diffusivity is negligible therefore the last term in Eq. (3.6) may be omitted. The convective term in the left-hang side is vanishing as well due to the divergence of  $c_m^p$  in the critical

neighborhood ( $c_s' \ll c_m^p$ ). Therefore, in the bulk, Eq. (3.6) may be written as

$$\rho_m' c_m^p \frac{d\delta T_{in}'}{dt'} = -\varphi \frac{T'}{\rho_f'} \left( \frac{\partial \rho_f'}{\partial T'} \right)_{P'} \frac{d\delta P'}{dt'} \quad (3.7)$$

where the variables  $T'$  and  $P'$  are replaced by  $\delta T'$  and  $\delta P'$ . In the left-hand side of Eq. (3.7), we mark  $\delta T'$  by the subscript "in" indicating that it is the temperature variation in the interior region. The pressure variation  $\delta P'$  in the right-hand side of Eq. (3.7) is substituted by the expression of Eq. (3.5) leading to the equation

$$\begin{aligned} \frac{d\delta T_{in}'}{dt'} &= \\ &= -\frac{\varphi}{\rho_f' (\rho_m' c_m^p) \rho_m' V'} \left( \frac{\partial \rho_f'}{\partial T'} \right)_{P'} \left( \frac{\partial P'}{\partial s_m'} \right)_{\rho_m'} \frac{d}{dt'} Q' \end{aligned} \quad (3.8)$$

The product of derivatives in Eq. (3.8) is replaced by

$$\begin{aligned} \left( \frac{\partial \rho_f'}{\partial T'} \right)_{P'} \left( \frac{\partial P'}{\partial s_m'} \right)_{\rho_m'} &= \\ &= \left( \frac{\partial \rho_f'}{\partial T'} \right)_{P'} \left( \frac{\partial P'}{\partial T'} \right)_{\rho_f'} \left( \frac{\partial T'}{\partial s_m'} \right)_{\rho_m'} \end{aligned} \quad (3.9)$$

where two first derivatives in the right-hand side are defined solely by the properties of fluid phase. Using the thermodynamic identity for fluids

$$\left( \frac{\partial P'}{\partial T'} \right)_{\rho_f'} \left( \frac{\partial \rho_f'}{\partial T'} \right)_{P'} = -\frac{\rho_f'^2 (c_p' - c_v')}{T'} \quad (3.10)$$

we have instead of Eq. (3.8) the equation

$$\frac{d\delta T_{in}'}{dt'} = \varphi \frac{\rho_f' (c_p' - c_v')}{(\rho_m' c_m^p) \rho_m' c_m' V'} \frac{dQ'}{dt'} \quad (3.11)$$

Equations (2.4) and (2.8) yield the identity

$$\varphi \rho_f' (c_p - c_v) = \rho_m' c_m^p - \rho_m' c_m' \quad (3.12)$$

transforming Eq. (3.11) to the form

$$\frac{d\delta T_{in}'}{dt'} = \frac{\rho_m' c_m^p - \rho_m' c_m'}{(\rho_m' c_m^p) \rho_m' c_m' V'} \frac{dQ'}{dt'} \quad (3.13)$$

Note, Eq. (3.13) contains solely the variables of porous medium.

The value  $J' = \frac{dQ'}{dt'}$  is the heat flux entering to the cell in a time unity which is related to the local heat flux (per surface unity)  $j'$  as  $j' = \frac{dJ'}{ds'}$ . The value  $j'$  is defined by the expression  $j' = -\lambda_m' \vec{n} \vec{\nabla} T'$  including the temperature gradient at the boundary  $\vec{\nabla} T'$  and the unity vector normal to the boundary  $\vec{n}$ . Combining the expressions of  $J'$  and  $j'$ , we have

$$J' = \lambda_m' \oint d\omega' |\vec{\nabla} T'| \quad (3.14)$$

and substituting Eq. (3.14) for Eq. (3.13), obtain

$$\frac{d\delta T_{in}'}{dt'} = \frac{\rho_m' c_m^p - \rho_m' c_m'}{(\rho_m' c_m^p) \rho_m' c_m' V'} \lambda_m' \oint d\omega' |\vec{\nabla} T'| \quad (3.15)$$

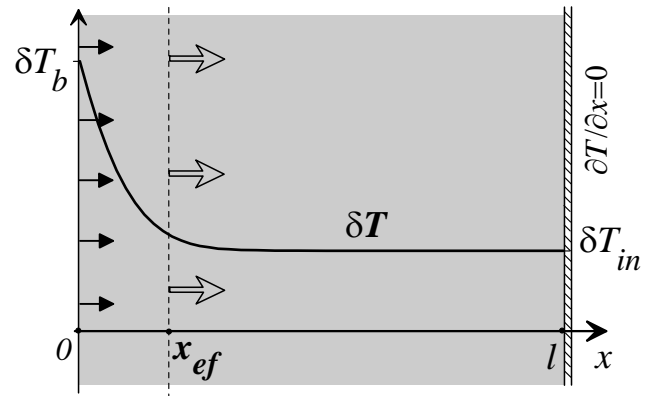


Fig. 1. Configuration of the piston effect in a layer.

Equation (3.15) relates temperature changes in the bulk region with temperature gradients at boundaries. Equation (3.15) is derived from Eq. (3.7) which neglects the thermal diffusion mechanism and takes into account only the work done by pressure. Consequently, Eq. (3.15) is responsible for an adiabatic temperature change called the piston effect.

Now we study the thermal response of medium to a step-temperature heat supply in an infinite layer shown in Fig. 1.

The temperature at the left boundary simultaneously rises in some value  $\delta T_b'$  and is fixed. The right boundary is thermally insulated.

The module of temperature gradient near the heated wall  $|\bar{\nabla}T'|$  is related to the temperature step  $\delta T_b'$  as  $|\bar{\nabla}\delta T'| \sim \delta T_b'/x_{ef}'$ . The length of boundary layer  $x_{ef}'$  increases in time due to thermal diffusion as  $x_{ef}' \sim 2\sqrt{D_m^{p'}t'}$  where  $D_m^{p'} = \frac{\lambda_m'}{\rho_m'c_m^{p'}}$  is the thermal diffusion coefficient.

Substituting the last relations for Eq. (3.15), we find

$$\frac{d\delta T_{in}'}{dt'} \approx \frac{\rho_m'c_m^{p'} - \rho_m'c_m'}{(\rho_m'c_m^{p'})\rho_m'c_m'l'} \lambda_m' \frac{\delta T_b'}{2\sqrt{D_m^{p'}t'}} \quad (3.16)$$

The time integral of Eq. (3.16) gives the temperature variation in the bulk:

$$\delta T_{in}' \approx \frac{(\rho_m'c_m^{p'} - \rho_m'c_m')\sqrt{\lambda_m'}}{l'\rho_m'c_m'\sqrt{\rho_m'c_m^{p'}}} \sqrt{t'} \delta T_b' \quad (3.17)$$

The characteristic time of the piston effect  $\tau_{pe}'$  is defined as the instant when the bulk temperature variation becomes near the temperature step at the boundary, i.e.  $\delta T_{in}' \approx \delta T_b'$ . This criterion gives instead of Eq. (3.17) the relation:

$$1 \approx \frac{\rho_m'c_m^{p'} - \rho_m'c_m'}{\rho_m'c_m'l'} \sqrt{\frac{\lambda_m'}{\rho_m'c_m^{p'}}} \sqrt{\tau_{pe}'} \quad (3.18)$$

and, at last, the expression of  $\tau_{pe}'$ :

$$\tau_{pe}' = \frac{(\rho_m'c_m')^2 \rho_m'c_m^{p'}l'^2}{(\rho_m'c_m^{p'} - \rho_m'c_m')^2 \lambda_m'} \quad (3.19)$$

Note, the heat capacities of porous medium  $c_m'$  and  $c_m^{p'}$  in Eq. (3.19) are determined in combination with the density  $\rho_m'$ . The products  $\rho_m'c_m'$  and  $\rho_m'c_m^{p'}$  are defined by Eqs. (2.4) and (2.8). We write Eq. (3.19) as an exact equalization since it is used for the definition of  $\tau_{pe}'$ . A validation of the definition of  $\tau_{pe}'$  by Eq. (3.19) will be done in the next subsection.

One can exhibit that Eq. (3.19) is simplified to the expression of the time of the piston effect in a single-phase fluid  $(\tau_{pe}')_f$  found in Ref. 13

$$(\tau_{pe}')_f = \frac{c_v'^2 c_p' \rho_f' l'^2}{(c_v' - c_p')^2 \lambda_f'} \quad (3.20)$$

if the porosity goes to the unity:  $\phi \rightarrow 1$  (the fraction of solid phase becomes negligible) and parameters of porous medium are replaced with parameters of pure fluid:  $\rho_m' \rightarrow \rho_f'$ ,  $c_m' \rightarrow c_v'$ ,  $c_m^{p'} \rightarrow c_p'$ ,  $\lambda_m' \rightarrow \lambda_f'$ .

With approach to the critical point, the complex  $\rho_m'c_m^{p'}$  becomes much greater than  $\rho_m'c_m'$  due to the divergence of  $c_m^{p'}$ . It leads to the tendency  $\tau_{pe}' \rightarrow \frac{(\rho_m'c_m')^2 l'^2}{\rho_m'c_m^{p'}\lambda_m'} \rightarrow 0$  which is similar to  $(\tau_{pe}')_f \rightarrow 0$  in a single-phase fluid.

### 3.2. NUMERICAL SIMULATIONS

A vertical rectangular cavity of porous material filled with a near-critical fluid in weightlessness ( $\bar{g} = 0$ ) is considered. The temperature is constant. The density of fluid phase is critical. The velocity is zero. At the initial moment, the temperature at the left boundary instantaneously rises in  $\Theta$  and is fixed. The other boundaries are thermally insulated.

The calculations were performed in a cavity at the aspect ratio  $h/l = 2$  on a nonuniform 81x81 grid. The initial temperature distance to the critical point  $T_i' - T_c'$  varies. The other parameters are:  $\Theta = 3.30 \cdot 10^{-5}$ ,  $\gamma_0 = 1.33$ ,  $Re = 3.97 \cdot 10^5$ ,  $Da = 4 \cdot 10^{-9}$ ,  $Pr_0 = 1.21 \cdot 10^{-2}$ ,  $M = 10^{-3}$ ,  $\phi = 0.4$ ,  $\rho_s c_s = 8.68$ ,  $\lambda_0 = 2.46 \cdot 10^{-2}$ ,  $\Lambda = 0.028$ ,  $\psi = 0.74$ . The dimensionless parameters characterize the cavity of length  $l' = 0.1$  m willed with CO<sub>2</sub> ( $T_c' = 304.15$  K,  $\rho_c' = 4.68 \cdot 10^2$  kg/m<sup>3</sup>,  $P_c' = 7.387$  MPa)<sup>1</sup> at  $\eta_0' = 32.57 \cdot 10^{-6}$  Pa·s,  $c_{v0}' = 567$  J/(kg·K),  $\lambda_0' = 0.05$  W/(m·K). The solid matrix is made of a sand-like matter at  $c_s' = 960$  J/(kg·K),  $\rho_s' = 2400$  Kg/m<sup>3</sup>,  $\lambda_s' = 3.35$  W/(m·K). At the initial moment, the temperature is 0.55 K above the critical one. Heating of the left boundary is in 0.01 K. The time step of integration varied in the range  $4.31 \cdot 10^{-4} \div 1.73 \cdot 10^{-2}$  s. In weightlessness, the problem is near to one-dimensional one.

In the case of a single-phase fluid, an analytical analysis<sup>13</sup> gives that the interior temperature deviation

$(\delta T_{in}')_f$  can be written in the following scaling form for  $t' \ll l^2/D'$  ( $D'$  is the thermal diffusion coefficient of pure fluid)

$$(\delta T_{in}')_f = \delta T_b' [1 - F_a(t'/(\tau_{pe}')_f)] \quad (3.21)$$

where  $F_a(s)$  is defined by  $F_a(s) = \exp(s)[1 - \text{erf}(\sqrt{s})]$  with  $\text{erf}(\sqrt{s})$  being the error function. As following from Eq. (3.21),  $(\delta T_{in}')_f / \delta T_b' = 0.572$  at  $t' = (\tau_{pe}')_f$  that is, at the instant to be equal to the time of the piston effect, the ratio of the interior temperature deviation to the boundary temperature step reaches 0.572. We apply this prediction to the piston effect in a porous layer and take from numerical simulations the instant  $\tau'$  corresponding to  $\delta T_{in}' / \delta T_b' = 0.572$ . The time  $\tau'$  depending on the temperature distance to the critical point  $T_i' - T_c'$  at two values of porosities:  $\varphi = 0.4$  and  $\varphi = 0.7$  is shown in Fig. 2.

For comparison, we show the analytical time of the piston effect defined by Eq. (3.19). For the fluid phase being the gas of van der Waals, Eq. (3.19) transforms into the form:

$$\tau_{pe}' = \frac{\rho_c' c_{v0}' l^2}{\lambda_{m0}'} \cdot \left( \frac{\varepsilon}{1+\varepsilon} \right)^2 \left( \frac{1}{\gamma_0 - 1} \right)^2 \cdot \frac{\sigma^2 \left( \sigma + \varphi(\gamma_0 - 1) \frac{1+\varepsilon}{\varepsilon} \right)}{\varphi^2 (1 + \varphi \lambda_0 \Lambda \varepsilon^{-\psi})} \quad (3.22)$$

The diffusive time  $\tau_d'$  is calculated analytically as well. The value of  $\tau_d'$  is defined by the problem on the propagation of temperature step in a moveless medium which has the solution<sup>25</sup>:  $\delta T' = \Theta'(1 - \text{erf}(0.5x'/\sqrt{D_m't'}))$ , here  $D_m' = \lambda_m' / (\rho_m' c_m')$ . The time  $\tau_d'$  is taken to be the instant when the ratio of the temperature increment at the right boundary  $\delta T'$  to the temperature step  $\Theta'$  reaches the chosen value of 0.572. This condition yields the constant  $C$ . We have:

$$\tau_d' = Cl^2 / D_m', \quad C = 0.393 \quad (3.23)$$

The dependency of  $\tau_d'$  on  $T_i' - T_c'$  at  $\varphi = 0.4$  and  $\varphi = 0.7$  is shown in Fig. 2.

At the end, we plot the curve of the time  $(\tau_{pe}')_f$  in a single-phase fluid defined by Eq. (3.20) which for the van der Waals gas may be reduced to the formula:

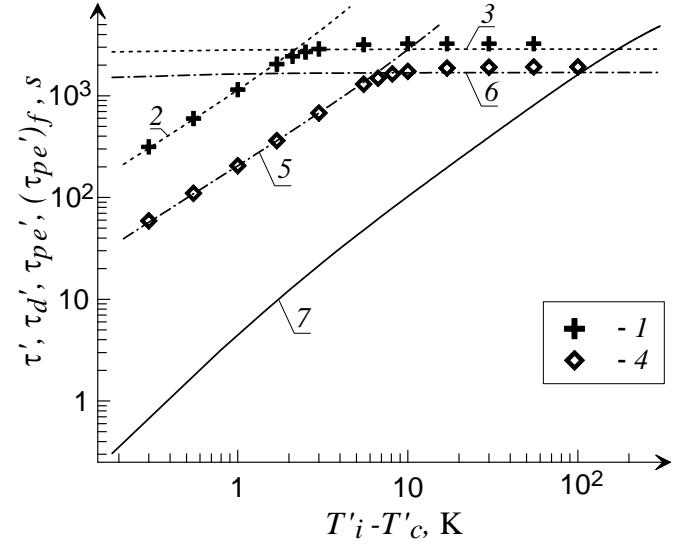


**Fig. 2.** Simulated time  $\tau'$  (1),  $\tau_{pe}'$  calculated by Eq. (3.22) (2),  $\tau_d'$  calculated by Eq. (3.23) (3) at  $\varphi = 0.4$ , and times  $\tau'$  (4),  $\tau_{pe}'$  (5),  $\tau_d'$  (6) at  $\varphi = 0.7$ . Time  $(\tau_{pe}')_f$  in a single-phase fluid calculated by Eq. (3.24) (7).

$$(\tau_{pe}')_f = \frac{\rho_c' c_{v0}' l^2}{\lambda_{m0}'} \cdot \left( \frac{\varepsilon}{1+\varepsilon} \right)^2 \left( \frac{1}{\gamma_0 - 1} \right)^2 \cdot \frac{\left( 1 + (\gamma_0 - 1) \frac{1+\varepsilon}{\varepsilon} \right)}{(1 + \Lambda \varepsilon^{-\psi})} \quad (3.24)$$

The value  $\varepsilon_i + 0.5\Theta$  is taken as  $\varepsilon$  in Eqs. (3.22) and (3.24).

As is clear from Fig. 2, at  $T_i' - T_c' > 2$  K for  $\varphi = 0.4$  and  $T_i' - T_c' > 7$  K for  $\varphi = 0.7$ , the simulated time  $\tau'$  is nearly independent of  $T_i' - T_c'$  and close to the value  $\tau_d'$  demonstrating the thermal diffusion mechanism to be dominant in thermal relaxation. With approach to the critical point, the time  $\tau'$  becomes shorter and shorter and is very near to  $\tau_{pe}'$  showing that the piston effect occurs and dominates. If the fraction of fluid phase is reduced (the porosity  $\varphi$  decreases), the range of temperature near the critical point responsible for the piston effect shortens, the piston effect slows down, and the curve of  $\tau_{pe}'$  goes away from that of  $(\tau_{pe}')_f$ .

Slowing down of the piston effect with decreasing in porosity may be explained as followed. During adiabatic heating, a fluid in the interior region gives up a part of energy

to the solid matrix since the phases are in local equilibrium and must have equal temperatures. Therefore only a part of work done by pressure in the boundary layer is consumed to heat a fluid in the bulk. In a medium at a lower porosity, the bigger part of energy is given up to the matrix to result in slowing down of the piston effect.

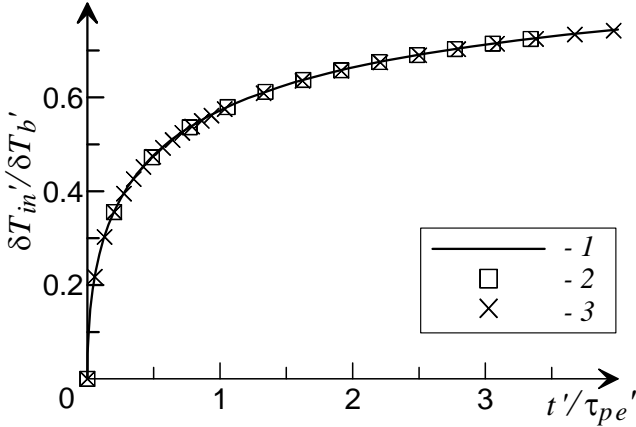


**Fig. 3.** Dependency of  $\delta T_{in}' / \delta T_b'$  on  $t' / \tau_{pe}'$  found analytically<sup>13</sup> (1), and by simulations at  $\phi = 0.4$ ,  $T_i' - T_c' = 0.55$  K (2), at  $\phi = 0.7$ ,  $T_i' - T_c' = 1.70$  K (3).

As mentioned above, the interior temperature deviation  $(\delta T_{in}')_f$  in a single-phase fluid satisfies Eq. (3.21) found in Ref. 13. One can show that the solution of the energy equation in a porous medium is the same and different solely in the time scale. To apply Eq. (3.21) to a porous layer, the time scale  $(\tau_{pe}')_f$  should change by  $\tau_{pe}'$ . The dependency of  $\delta T_{in}' / \delta T_b'$  on the scaled time  $t' / \tau_{pe}'$  is exhibited in Fig. 3. The results of numerical simulations at two sets of  $\phi$  and  $T_i' - T_c'$  (other parameters as above) are plotted in Fig. 3 as well. As is evident, the analytical and numerical results are in good agreement that validates the definition of  $\tau_{pe}'$  by Eq. (3.19) and demonstrates the applicability of Eq. (3.21) to near-critical porous layers.

We studied enhancing in the heat exchange by the piston effect and calculated the coefficient  $C = q / q_d$  shown in Fig.

4. Here  $q = -\int_0^h \lambda_m \partial T / \partial x dy$  is the heat flux at the heated boundary, and  $q_d$  is the same function at the zeroth velocity.

The value  $q$  characterizes the heat consumption by a cell due to the piston effect and thermal diffusion, whereas  $q_d$  only

due to thermal diffusion. Four sets of  $\phi$  and  $T_i' - T_c'$  are used at the above other parameters. If  $C > 1$ , enhancing of heat consumption due to the piston effect is observed. It is clear, that the piston effect is able to give a multiple enhancing of heat consumption at an initial time interval. Going to the critical point and increasing  $\phi$ , the action of the piston effect becomes more substantial while the time of this action shortens.

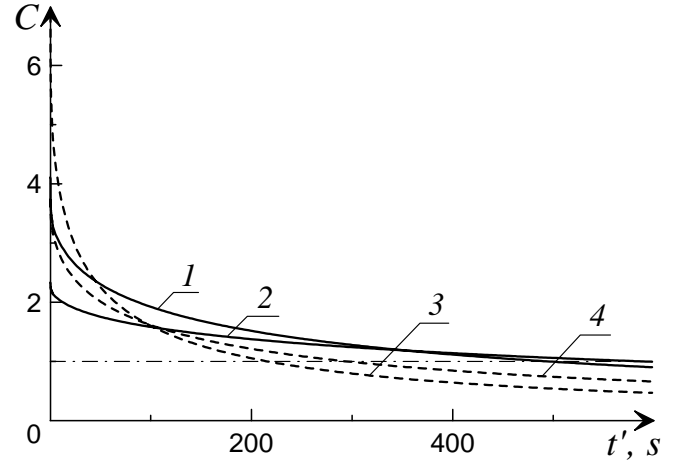


**Fig. 4.** Coefficient  $C$  depending on  $t'$  at  $\phi = 0.4$  and  $T_i' - T_c' = 0.55$  K (1),  $T_i' - T_c' = 1.70$  K (2), at  $\phi = 0.7$  and  $T_i' - T_c' = 0.55$  K (3),  $T_i' - T_c' = 1.70$  K (4). Dot-dashed line corresponds to  $C = 1$ .

### 3.3. RESTRICTIONS OF THE MODEL

The phases are assumed to be in local thermal equilibrium. However, as shown above, the piston effect goes faster and faster with approach to the critical point. Therefore, one can come to conditions when the phases are not able to reach thermal equilibrium in a time scale to be of order of the characteristic time of the piston effect. In a fine-grained matrix, equilibrium can be achieved whereas the temperature of matrix made of big grains may not be as much as the quick changeable temperature of fluid phase. One can estimate the characteristic size of grains. For the sake of simplicity, grains are assumed to be spheres of equal diameter. Heating of a separated grain is described as<sup>26</sup>

$$m' c_s' \frac{\partial T_s'}{\partial t'} = 2 \pi d'^2 \lambda_f' \frac{T_f' - T_s'}{d'} \quad (3.25)$$

Here,  $m' = \frac{\pi d'^3}{6} \rho_s'$  and  $d'$  are the mass and diameter of sphere. The characteristic time of heating of sphere  $\tau_q'$  is defined by the relation  $\partial T_s' / \partial t' = (T_f' - T_s') / \tau_q'$  that in

combination with Eq. (3.25) gives the formula:  $\tau_q' = d'^2 \rho_s' c_s' / (12 \lambda_f')$ . For equilibrium to be achieved, the condition  $\tau_q' \ll \tau_{pe}'$  should be satisfied. This condition with the use of Eq. (3.19) leads to the expression:

$$\left(\frac{d'}{l'}\right)^2 \ll \frac{12 \lambda_f' (\rho_m' c_m')^2 \rho_m' c_m^p'}{\lambda_m' \rho_s' c_s' (\rho_m' c_m^p' - \rho_m' c_m')^2} \quad (3.26)$$

If the fluid phase obeys the van der Waals equation of state, the last expression combined with Eq. (3.22) may be transformed into the form:

$$\left(\frac{d'}{l'}\right)^2 \ll \frac{12 \lambda_f' \rho_c' c_{v0}'}{\lambda_{m0}' \rho_s' c_s'} \cdot \left(\frac{\varepsilon}{1+\varepsilon}\right)^2 \left(\frac{1}{\gamma_0 - 1}\right)^2 \cdot \frac{\sigma^2 \left(\sigma + \varphi(\gamma_0 - 1) \frac{1+\varepsilon}{\varepsilon}\right)}{\varphi^2 (1 + \varphi \lambda_0 \Lambda \varepsilon^{-\nu})} \quad (3.27)$$

For the medium at stated above parameters, the estimations by Eq. (3.27) give the following values. If  $\varphi = 0.4$ , we have  $d' \ll 3$  cm at  $\varepsilon = 10^{-2}$ ,  $d' \ll 1$  cm at  $\varepsilon = 10^{-3}$ , and  $d' \ll 0.3$  cm at  $\varepsilon = 10^{-4}$ . If  $\varphi = 0.6$ , we have  $d' \ll 2$  cm at  $\varepsilon = 10^{-2}$ ,  $d' \ll 0.7$  cm at  $\varepsilon = 10^{-3}$ , and  $d' \ll 0.2$  cm at  $\varepsilon = 10^{-4}$ . As is evident, for  $\varepsilon \geq 10^{-3}$ , the obtained values are realistic for many practical cases that validates the approach of local thermal equilibrium.

There are restrictions on a very small size of grains and pores (being of the same order). Tending to the critical point, the fluctuations in a fluid grow. The correlation length  $\xi'$  is described by the power-law relation:

$$\xi' = \xi_0' \varepsilon^{-\nu} \quad (3.28)$$

where  $\xi_0' = 10^{-8}$  cm and  $\nu = 2/3$  for a typical fluid<sup>27</sup>. A fluid phase can not be considered as a homogeneous continuous medium if the correlation length becomes of order of the size of pores. We obtain from this criterion that  $d' \gg 10^{-6}$  cm at  $\varepsilon = 10^{-3}$ , and  $d' \gg 5 \cdot 10^{-6}$  cm at  $\varepsilon = 10^{-4}$ . The finding estimations are satisfied in major cases.

## 4. CONVECTION IN SIDE-HEATED CELLS

### 4.1. CORRELATION RELATIONS

For problems of convection in pure fluids, the method of comparison of flows near and far from the critical point was developed<sup>15,28,29</sup>. Two fluids having analogous physical properties except the compressibility are compared allowing us to recognize effects of high compressibility, particularly, adiabatic heating near the critical point. To match the fluids, the correlation relations connecting the model (contained in the government equations) and real (actually characterizing convection) criteria of similarity were derived.

A similar method may be developed for porous media as well. Tending to the critical point, the heat capacity  $c_p'$ , the coefficients  $\beta'$  and  $\lambda_m'$  go to infinity whereas all dimensionless complexes defined by Eqs. (2.15) remain fixed. The permeability  $K'$  may also change in critical region but we do not have sufficient data on its behavior and assume the value  $K'$  to be constant. To characterize near-critical convection, one should define the real criteria of similarity containing the actual values of  $c_p'$ ,  $\beta'$ , and  $\lambda_m'$ . We write

$$Ra_d = \frac{\Theta' \beta' g' l' K' \rho_c'^2 c_p'}{\lambda_m' \eta'}, \quad Pr = \frac{c_p' \eta'}{\lambda_m'} \quad (4.1)$$

Substituting  $c_p'$  and  $\beta'$  by the thermodynamic identities

$$\beta' = -\frac{1}{\rho'} \left( \frac{\partial \rho'}{\partial T'} \right)_{P'}, \quad c_p' = c_v' + \frac{T'}{\rho'^2} \left( \frac{\partial P'}{\partial T'} \right)_{\rho'}^2 \left( \frac{\partial \rho'}{\partial P'} \right)_{T'}, \quad (4.2)$$

and transforming Eqs. (4.1), one can find

$$Ra_d = -Ra_{d0} \frac{K}{\lambda_m} \rho \left( \frac{\partial \rho}{\partial T} \right)_P \left( \frac{1}{\gamma_0} - \frac{\gamma_0 - 1}{\gamma_0} \frac{T}{\rho^2} \left( \frac{\partial P}{\partial T} \right)_{\rho} \left( \frac{\partial \rho}{\partial T} \right)_P \right)$$

$$Pr = Pr_0 \frac{1}{\lambda_m} \left( \frac{1}{\gamma_0} - \frac{\gamma_0 - 1}{\gamma_0} \frac{T}{\rho^2} \left( \frac{\partial P}{\partial T} \right)_{\rho} \left( \frac{\partial \rho}{\partial T} \right)_P \right) \quad (4.3)$$

The derivatives in Eqs. (4.3) are determined by the equation of state of fluid phase. For the van der Waals equation of state near the critical isochore, one can write

$$Ra_d = \frac{2}{3} Ra_{d0} \frac{K}{\lambda_m \varepsilon} \left( \frac{1}{\gamma_0} + \frac{\gamma_0 - 1}{\gamma_0} \cdot \frac{1 + \varepsilon}{\varepsilon} \right)$$

$$Pr = Pr_0 \frac{1}{\lambda_m} \left( \frac{1}{\gamma_0} + \frac{\gamma_0 - 1}{\gamma_0} \cdot \frac{1 + \varepsilon}{\varepsilon} \right) \quad (4.4)$$

Equations (4.4) connecting the model Rayleigh-Darcy  $Ra_{d0}$  and Prandtl  $Pr_0$  numbers with their real analogies  $Ra_d$  and  $Pr$  are called the correlation relations.

#### 4.2. NUMERICAL SIMULATIONS

A vertical rectangular porous cell filled with a near-critical fluid in the Earth's gravity field ( $\vec{g} = (0, -1)$ ) is considered. The temperature is constant, the velocity is zero, and the fluid is stratified. The density of fluid in the central plane of cell is critical. At the initial moment, the temperature at the left boundary instantaneously rises in  $\Theta$  and is fixed. The right boundary is held at the initial temperature while the horizontal boundaries are thermally insulated. The sketch of the problem is shown in Fig. 5. The matter of matrix is the same as in the previous section, the fluid phase is water ( $T_c' = 647.3$  K,  $\rho_c' = 3.21 \cdot 10^2$  kg/m<sup>3</sup>,  $P_c' = 22.12$  MPa)<sup>1</sup>. The near-critical physical properties of water are taken from e-Tables (<http://twt.mpei.ac.ru/ochkov/WSPHB/Engindex.html>) being the electronic appendix to Ref. 30. The initial temperature is 2 K above the critical one, the temperature step at the left boundary is 0.1 K.

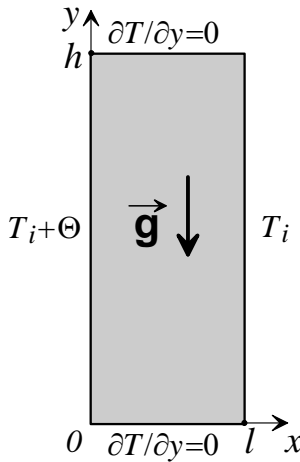


**Fig. 5.** Sketch of problem.

The calculations were performed in a cell at the length  $l' = 1$  m and aspect ratio  $h/l = 3$  on a nonuniform 61x81 grid. The dimensionless parameters are:  $\varepsilon_i = 3.09 \cdot 10^{-3}$ ,  $\Theta = 1.55 \cdot 10^{-4}$ ,  $\gamma_0 = 1.29$ ,  $Ra_{d0} = 5.64 \cdot 10^{-2}$ ,  $Re = 6.65 \cdot 10^6$ ,  $Da = 5 \cdot 10^{-12}$ ,  $Pr_0 = 6.50 \cdot 10^{-2}$ ,

$M = 10^{-3}$ ,  $\varphi = 0.4$ ,  $\rho_s c_s = 1.80$ ,  $\lambda_0 = 0.268$ ,  $\Lambda = 8.72 \cdot 10^{-3}$ ,  $\psi = 0.992$ . The time step of integration varied in the range  $1.31 \cdot 10^{-2} \div 2.10$  s.

For comparison, simulation in a cell with an ideal gas (obeying the equation of state:  $P = \rho T$ ) was performed. Convection of the near-critical fluid is characterized by the real Rayleigh-Darcy  $Ra_d$  and Prandtl  $Pr$  numbers which are calculated by Eqs. (4.4):  $Ra_d = 654$  and  $Pr = 3.58$ ; the value  $\varepsilon_i + 0.5\Theta$  is taken as  $\varepsilon$ . Since, in an ideal gas, the model and real criteria of similarity are equal to each other, simulation of convection in the ideal gas was carried out at  $Ra_{d0} = 654$  and  $Pr_0 = 3.58$  in the government equations. Growing in  $Ra_{d0}$  as compared with a near-critical fluid phase is provided by growing in  $\Theta$  to be equal to  $\Theta = 3.25 \cdot 10^{-2}$  in the case of ideal gas. The other parameters are as stated above.

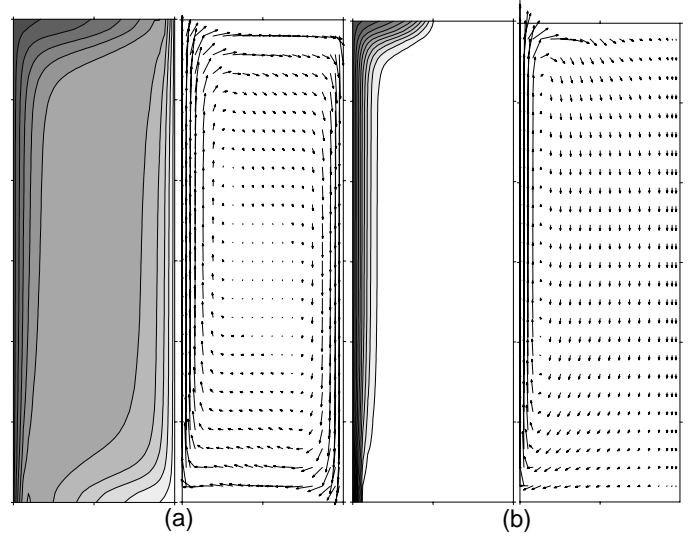


**Fig. 6.** Temperature and velocity fields in a porous cell with a near-critical fluid at  $Ra_{d0} = 5.64 \cdot 10^{-2}$  and  $Pr_0 = 6.50 \cdot 10^{-2}$  (a), and with an ideal gas at  $Ra_{d0} = 654$  and  $Pr_0 = 3.58$  (b) at the instant  $t' = 1.31 \cdot 10^5$  s.

Side heating initiates gravity-driven convection in a fluid phase. In Fig. 6, the field of isotherms defined by the variable  $(T' - T_i') / \Theta'$  and the dynamical field in two media at the instant corresponding to an unsteady regime of convection are demonstrated. In pictures with a gradient fill, the most dark color corresponds to the maximum value, and the white color to the minimum value. As is evident, in the near-critical fluid, two jets are formed whereas, in the ideal gas, a single jet rises near the heated boundary. This qualitative distinction is

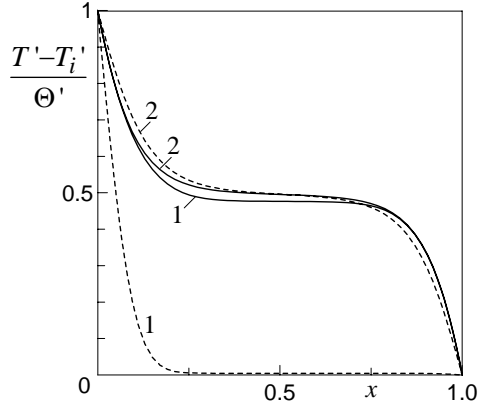


**Fig. 7.** Temperature increment  $(T' - T_i') / \Theta'$  in the central horizontal plane in a porous cell with a near-critical fluid at  $Ra_{d0} = 5.64 \cdot 10^{-2}$  and  $Pr_0 = 6.50 \cdot 10^{-2}$  (solid lines), and with an ideal gas at  $Ra_{d0} = 654$  and  $Pr_0 = 3.58$  (broken lines) at the instant  $t' = 1.31 \cdot 10^5$  (1);  $1.70 \cdot 10^7$  (2) s.

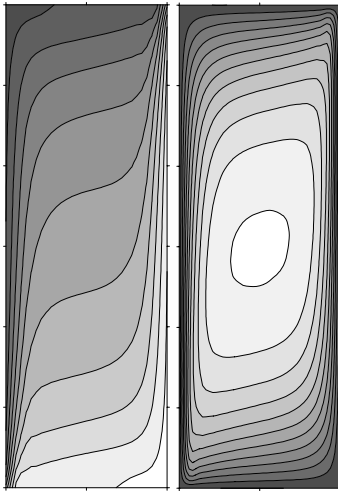


**Fig. 8.** Fields of temperature and stream function in a porous cell with a near-critical fluid at  $Ra_{d0} = 5.64 \cdot 10^{-2}$  and  $Pr_0 = 6.50 \cdot 10^{-2}$  in steady-state convection.

associated with the piston effect in the first case. The time of the piston effect  $\tau_{pe}' = 2.25 \cdot 10^4$  s is a several times shorter than the demonstrated instant  $t' = 1.31 \cdot 10^5$  s therefore the piston effect manages to heat an interior region of cell forming the cool boundary layer near the right (isothermal) wall. As a result, a jet moving down is formed near the right wall while the other jet rises near the left (heated) wall. In an ideal gas, a single boundary layer is formed due to conductivity near the

heated boundary initiating a single jet. The temperature profiles are shown in Fig. 7; see curves 1.

For a long time over the diffusive time  $\tau_d'$ , the steady-state regime of convection is reached and the role of the piston effect is anticipated to become negligible. In Fig. 7, the temperature profiles at the instant  $t' = 1.70 \cdot 10^7$  s exceeding the time  $\tau_d' \approx 6 \cdot 10^5$  s in media with a near-critical fluid and an ideal gas are drawn; see curves 2. As is evident, the temperature profiles are close to each other indicating the similarity of thermal fields in two media. In Fig. 8, the temperature field and field of stream function in steady-state regime are shown; the patterns of an ideal gas are very near and therefore not exhibited. In steady conditions, circular one-roll motions both in a near-critical fluid and an ideal gas are observed.

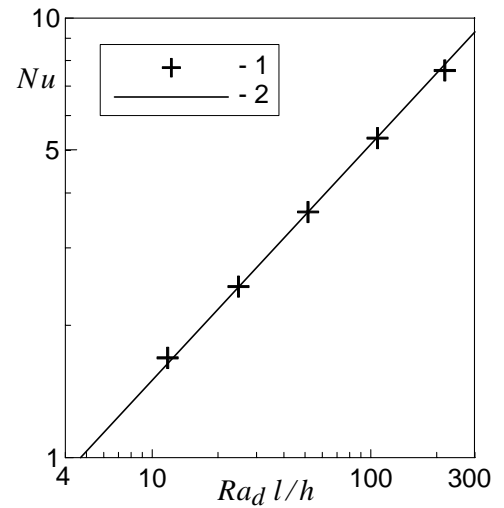


**Fig. 9.** Dependence of  $Nu$  on  $Ra_d l/h$  in a vertical cell at the aspect ratio  $l/h = 3$  obtained by simulations (1) and analytically<sup>31</sup> (2).

To characterize the convective heat transfer, the Nusselt number  $Nu$  at the side boundaries was calculated by the equation:  $Nu = -1/j \int_0^h \lambda_m \partial T / \partial x dy$ , here  $j$  is heat flux in

a moveless medium. In a steady-state regime, the Nusselt numbers at the left and right walls are equal to each other. The initial value  $\varepsilon_i$  varies so that we have the variation of the real Rayleigh-Darcy number  $Ra_d$  at the fixed model number  $Ra_{d0}$ . The dependences of  $Nu$  on the complex  $Ra_d l/h$  at the aspect ratio  $h/l = 3$  are shown in Fig. 9. The variations of  $\varepsilon_i$  are corresponding to  $T_i' - T_c' = 2 \div 10$  K. The other parameters are as stated in the beginning of this section.

The problem of steady-state convection in vertical porous layers at a fixed temperature difference at boundaries was solved analytically<sup>31</sup> for a low compressible liquid phase. The solution<sup>31</sup> was obtained in an approach of no interplay between thermal boundary layers but taking into account the limited height of cell. The analytical dependence  $Nu(Ra_d l/h)$  at  $h/l=3$  is demonstrated in Fig. 9. As is clear, the numerical and analytical data are in good agreement indicating two important consequences. First, the agreement of data validates the use of the correlation relations defined by Eq. (4.4). Second, this result demonstrates that the heat transfer in a layer with a high compressible fluid phase is the same as in a layer with a low compressible fluid phase that is the effects of high compressibility, particularly, adiabatic heating are negligible in steady-state convection.

## 5. CONVECTION IN BOTTOM-HEATED CELLS

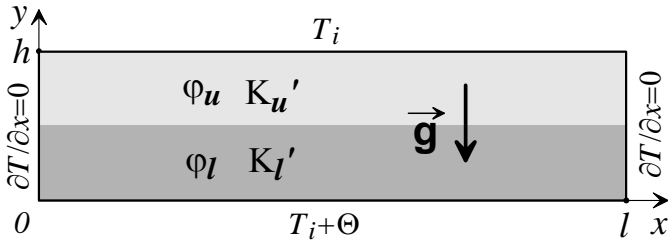


Fig. 10. Sketch of problem.

A horizontal rectangular porous cell filled with a near-critical fluid in terrestrial gravity ( $\vec{g} = (0, -1)$ ) is considered. The cell consists of two horizontal contacting layers of different porosity and permeability. We assign the porosity  $\varphi_l$  and permeability  $K_l'$  to a lower layer whereas  $\varphi_u$  and  $K_u'$  to an upper layer. The system is isothermal, the fluid is moveless and stratified. The fluid density reaches the critical value in the central plane of cell. At the initial moment, the temperature at the bottom instantaneously rises in  $\Theta$  and is fixed. The top boundary is held at the initial temperature. The vertical boundaries are thermally insulated. The sketch of the problem is shown in Fig. 10.

The porous layers are made of the same matter therefore the permeability is related to the porosity. We take  $\varphi_l = 0.4$ ,  $\varphi_u = 0.6$ , and  $K_l' = 4 \cdot 10^{-11} \text{ m}^2$  and calculate  $K_u'$  from the dependence<sup>22</sup> simplified in the case of grains of equal diameters to the form

$$\frac{K_l'(1-\varphi_l)^2}{\varphi_l^3} = \frac{K_u'(1-\varphi_u)^2}{\varphi_u^3} \quad (5.1)$$

We obtain  $K_u' = 3.04 \cdot 10^{-10} \text{ m}^2$ . The cell has the height  $h' = 0.1 \text{ m}$  and the aspect ratio  $l/h = 4$ . The Darcy numbers at the bottom and top normalized by  $h'$  are  $Da_l = 4 \cdot 10^{-9}$  and  $Da_u = 3.04 \cdot 10^{-8}$ , respectively.

The solid matter is as in the previous sections. The fluid is  $\text{CO}_2$ . The initial temperature is  $0.55 \text{ K}$  above the critical one. The temperature step is  $6.08 \cdot 10^{-3} \text{ K}$ . The other dimensionless parameters (normalized by  $h'$ ) are:  $\varepsilon_i = 1.81 \cdot 10^{-3}$ ,  $\Theta = 2.00 \cdot 10^{-5}$ ,  $\gamma_0 = 1.33$ ,  $\text{Re} = 3.97 \cdot 10^5$ ,  $\text{Pr}_0 = 1.21 \cdot 10^{-2}$ ,  $M = 10^{-3}$ ,  $\rho_s c_s = 8.68$ ,  $\lambda_0 = 2.46 \cdot 10^{-2}$ ,  $\Lambda = 0.028$ ,  $\psi = 0.74$ .

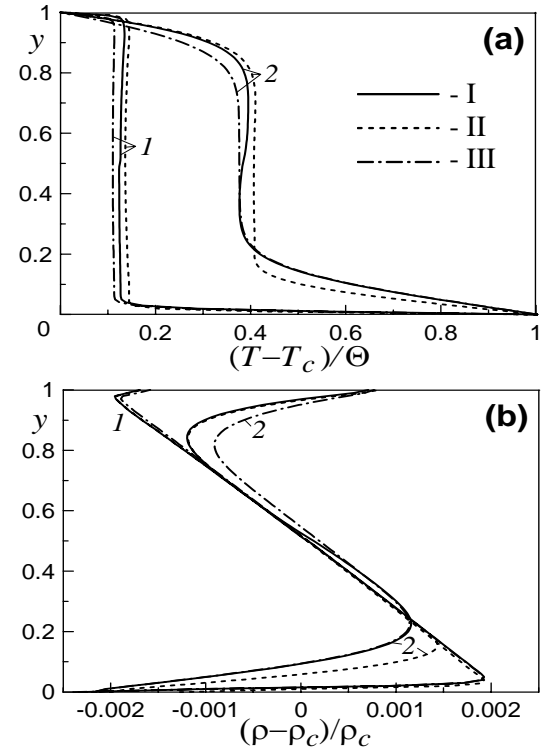
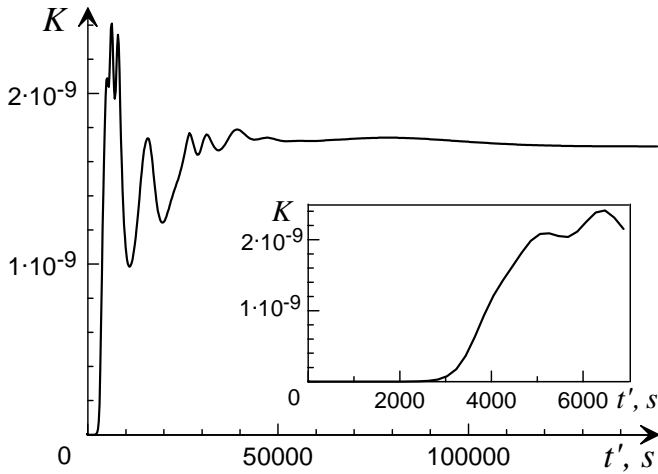


Fig. 11. Temperature profiles  $(T - T_c)/\Theta$  (a) and density profiles  $(\rho - \rho_c)/\rho_c$  (b) along the central vertical line in a two-layer porous matrix at  $\varphi_l = 0.4$ ,

$Da_l = 4 \cdot 10^{-9}$ ,  $\varphi_u = 0.6$ , and  $Da_u = 3.04 \cdot 10^{-8}$  (I) and in a uniform matrix at  $\varphi = 0.6$  and  $Da = 3.04 \cdot 10^{-8}$  (II), at  $\varphi = 0.4$  and  $Da = 4 \cdot 10^{-9}$  (III) at the instants  $t' = 10.1$  (1), and 592 (2) s.

The problem under study is of interest with respect to the complexity of dynamic phenomena. In short times, the piston effect goes in a fluid phase. As obtained in Section 3, the

characteristic time  $\tau_{pe}'$  depends on the porosity leading to the different values of  $\tau_{pe}'$  in lower and upper halves of cell. The fluid phase is subjected to hydrostatic effects. The features of the piston effect in variable conditions (determined by different  $\tau_{pe}'$ ) in a gravity field are of interest in the initial stage of process. In longer time intervals, a fluid starts to convect. The real Rayleigh-Darcy number  $Ra_d$  depends on the permeability therefore convection is characterized by different values of  $Ra_d$  in lower and upper parts of cell. A start of convection, peculiarities of convective flows and heat transfer in variable conditions (determined by different  $Ra_d$ ), and convective structures in a steady-state regime are of interest in following stages of process.



**Fig. 12.** Dependence of the kinetic energy  $K$  on the time  $t'$ .  
Insert: the same dependence in a shortened time interval.

At the initial instant, bottom heating is turned on to initiate the piston effect in a fluid phase. To recognize an influence of two-layer porous matrix on the piston effect, two additional problems associated with a uniform container were solved numerically. In second case, a matrix has parameters  $\varphi = 0.6$  and  $Da = 3.04 \cdot 10^{-8}$  to be the same as in the upper part of two-layer cell. In third case, the parameters are  $\varphi = 0.4$  and  $Da = 4 \cdot 10^{-9}$  as in the lower part of that. The time of the piston effect calculated by Eq. (3.22) is  $\tau_{pe}' = 198$  s in the second problem and  $\tau_{pe}' = 592$  s in third one corresponding to the values of  $\tau_{pe}'$  at the upper and lower parts of cell under study. In the absence of convection, thermal and dynamic patterns are nearly one-dimensional. The temperature and density profiles across the cell are shown in Fig. 11. As is clear, the temperature and density profiles deflect from each other a little despite an essential difference

in values of  $\tau_{pe}'$ . Nevertheless, some differences are observed and, at the instant  $t' = 592$  s (curves 2), the profiles of  $(T - T_c)/\Theta$  and  $(\rho - \rho_c)/\rho_c$  in a two-layer container approach at the top to the profiles in second case and at the bottom to those in third case. The fluid phase is stratified and, as exhibited in Fig. 11 (b), stratification is retained in the interior region of cell during the action of the piston effect in all cases.

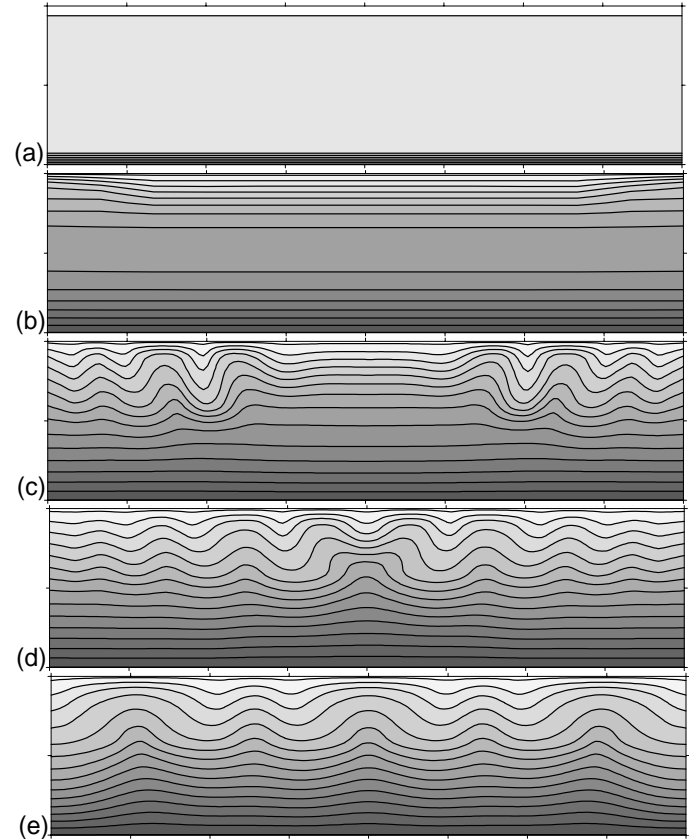


**Fig. 13.** Field of temperature at the instants  $t' = 10.1$  (a),  $3.63 \cdot 10^3$  (b),  $6.65 \cdot 10^3$  (c),  $9.65 \cdot 10^3$  (d),  $5.10 \cdot 10^5$  (e) s.

We calculated the normalized kinetic energy of fluid  $K$  by the equation:  $K = \frac{1}{hl} \int_0^h \int_0^l \frac{\rho \vec{U}^2}{2} dx dy$ . The value of  $K$  is nearly zero for a some time and starts to grow with convection to develop. As shown in Fig. 12 (insert), the energy  $K$  starts to grow at the instant about  $3 \cdot 10^3$  s substantially exceeding the characteristic times of the piston effect in the lower and upper parts of cell but being shorter than the diffusive time  $\tau_d' = 7.12 \cdot 10^3$  s. The comparison of characteristic times

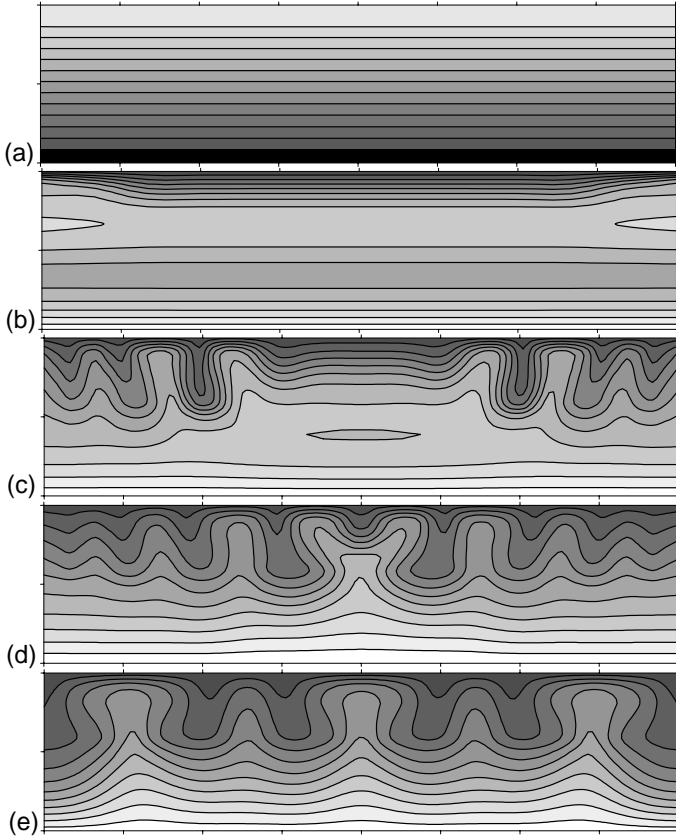


**Fig. 14.** Field of density at the instants as in Fig. 13.

shows that convection starts when the piston effect nearly finished however a diffusive mechanism did not manage to fit the temperature field generated by the piston effect. It means that the fluid phase starts to convect in the thermal field remembering the piston effect. As is clear from Fig 12, at the initial stage of convection, the curve of  $K$  oscillates resulted from changing of convective patterns. Later, a steady-state regime of convection is reached associating with the energy  $K$  to approach to constant.

To demonstrate a structure of convection at different time instants, we show the thermal field in Fig. 13, the field of density in Fig. 14, and the field of gradient of density in Fig. 15. The gradient of density was calculated as the function  $f = \left\{ (\partial \rho / \partial x)^2 + (\partial \rho / \partial y)^2 \right\}^{1/2}$  then the field of  $f$  was plotted in Fig. 15. We see from Figs. 13-15 (a), (b) that due to heating of interior region by the piston effect in the initial stage, two boundary layers (hot one near the bottom and cold one near the top) are formed. The gradient of density reaches highest values near the top corners of cell (Fig. 15 (b)) resulting to a grow of instabilities. Later, cold plumes moving down are generated near the top boundary (Figs. 13-15 (c)). The top boundary layer is disturbed initially near the vertical walls then closer to its center. Note that instabilities in the Rayleigh-Benard configuration were analyzed numerically in the case of

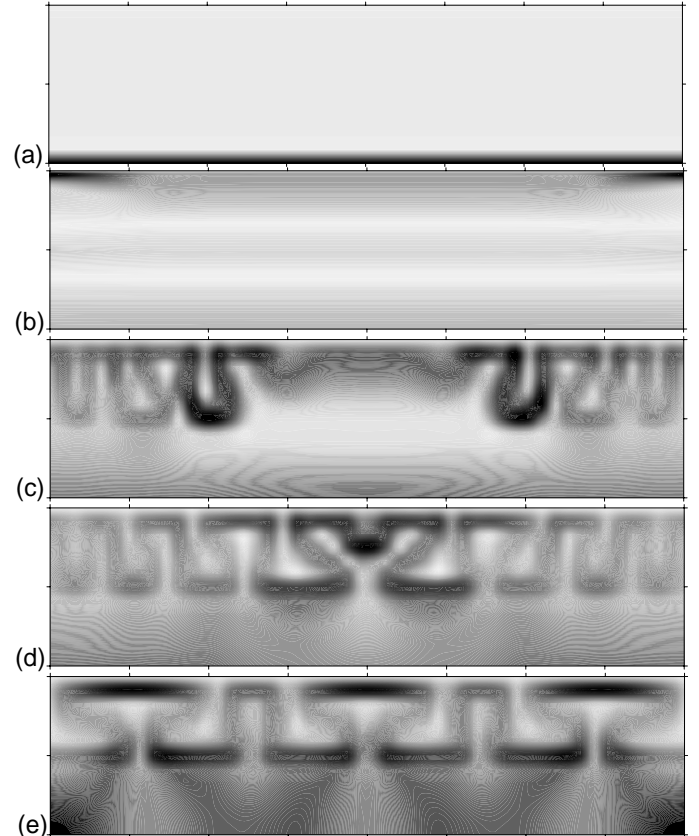


**Fig. 15.** Field of density gradient at the instants as in Fig. 13.

a pure near-critical fluid<sup>32</sup>. The analysis<sup>32</sup> showed that the top and bottom boundary layers were disturbed nearly simultaneously generating downward and upward thermal plums. In the present study, instabilities are generated only near the top that may be explained by different characteristics of convection below and above. As the lower and upper porous matrixes have different values of permeability  $K_l'$  and  $K_u'$ , respectively, the values of the model (see Eq. (2.15)) and, consequently, real (see Eq. (4.4)) Rayleigh-Darcy numbers are different as well. We obtain the values of the real Rayleigh-Darcy number  $Ra_d = 95.6$  at the bottom and  $Ra_d = 716$  at the top. Since the upper number  $Ra_d$  is an order of magnitude higher than the lower one, inhomogeneities are observed near the top wall. In a time interval associated with the onset of convection near the top wall, inhomogeneities near the bottom wall do not manage to originate.

In a longer time, a convective motion covers the whole upper half of cell and penetrates the lower half (Figs. 13-15 (d)). Finally, a steady-state regime of convection is reached (Figs. 13-15 (e)) characterizing by a periodic convective structure most clearly exhibited by the gradient of density (Fig. 15 (e)). We see three big plumes and two small plumes in between rising from the lower porous layer to the top. The

upward plumes alternate with downward plumes moving from the top. The highest values of the gradient of density are observed near the top wall and at the interface of porous layers due to deceleration of plumes. A convective heat transfer in a steady-state regime is characterized by the Nusselt number  $Nu = 1.47$  to be the same at the bottom and top walls.

## 6. CONCLUSIONS

In this paper, a thermodynamic analysis of the piston effect (adiabatic heating) stimulated by the step-temperature heat supply in a porous layer filled with a near-critical fluid was carried out. The dependence of the characteristic time of the piston effect on properties of fluid and solid phases was found. We examined by simulation the dependence of bulk temperature rise on time for a single-phase fluid<sup>13</sup> and obtained that this function for a porous medium is the same but over a different time scale (the characteristic time of the piston effect in a porous medium is used instead of that in a single-phase fluid).

To recognize an influence of the piston effect on gravity-driven convection, the correlation relations connecting the model (set into the government equations) and real (characterizing convection actually) Rayleigh-Darcy and Prandtl numbers were written. The use of the correlation relations allowed us to compare dynamics and heat transfer in porous media filled with a near-critical fluid and a perfect gas to have analogous physical properties except a high compressibility. Comparing the results of simulation in vertical rectangular cells with side heating, it was shown that, in an unsteady regime, the piston effect can change convective patterns qualitatively but, in a steady-state regime, there is an analogy in the heat transfer in two cases since the piston effect is negligible.

Simulations of the piston effect, the onset and development of convection in a cell heated from below were carried out. We considered a complex problem associated with a two-layer porous matrix and characterized by two sets of porosity, permeability, characteristic time of the piston effect, and Rayleigh-Darcy number. It was exhibited that, during the piston effect, stratification of fluid phase in the interior region retains and the temperature and density profiles do not change significantly depending on porosity and permeability. However, the onset and development of convection depend on properties of matrix significantly. As found, inhomogeneities are generated in the top boundary layer despite the cell is heated from below. Convection in a steady-state regime has a complex periodic structure resulted from the most motion to concentrate on the upper half of cell.

## ACKNOWLEDGMENTS

The author is indebted to Professor V.I. Polezhaev for helpful discussions. This work was funded by the Russian Foundation for Basic Research (Grant 07-08-00188) and the Program of the Leading Scientific School (Grant 3066.2006.8).

## REFERENCES

- [1] M.A. Anisimov, "Critical Phenomena in Liquids and Liquid Crystals." Gordon and Breach, Philadelphia (1991).
- [2] R. De Brjin, R.J.J. Van Diest, T.D. Karapantsios, A.C. Michels, W.A. Wakeham, & J.P.M. Trusler, "Heat Transfer in Pure Critical Fluids Surrounded by Finitely Conducting Boundaries in Microgravity." *Physica A* **242**: 119-140 (1997).
- [3] R.A. Wilkinson, G.A. Zimmerli, H. Hao, M.R. Moldover, W.L. Johnson, R.A. Ferrel, & R.W. Gammon, "Equilibration near the liquid-vapor critical point in microgravity." *Phys. Rev. E* **57**(1): 436-448 (1998).
- [4] Y. Garrabos, M. Bonetti, D. Beysens, F. Perrot, T. Fröhlich, P. Carlès, & B. Zappoli, "Relaxation of a Supercritical Fluid after a Heat Pulse in the Absence of Gravity Effects: Theory and Experiments." *Phys. Rev. E* **57**(5): 5665-5681 (1998).
- [5] A. Haupt, & J. Straub, "Evaluation of Isochoric Heat Capacity Measurements at the Critical Isochore of SF<sub>6</sub> Performed during the German Spacelab Mission D-2." *Phys. Rev. E* **59**(2): 1795-1802 (1999).
- [6] A.V. Zyuzgin, A.I. Ivanov, V.I. Polezhaev, G. F. Putin, & E.B. Soboleva, "Convective Motions in Near-Critical Fluids under Real Zero-Gravity Conditions." *Cosmic Research* **39**(2): 175-186 (2001).
- [7] H. Azuma, Sh. Yoshihara, M. Onishi, K. Ishii, Sh. Masuda, & T. Maekava, "Natural Convection Driven in CO<sub>2</sub> Near its Critical Point under Terrestrial Gravity Conditions." *Int. J. Heat Mass Transfer* **42**(4): 771-774 (1999).
- [8] A. B. Kogan, & H. Meyer, "Heat Transfer and Convection Onset in a Compressible Fluid: <sup>3</sup>He Near the Critical Point." *Phys. Rev. E* **63**: paper 056310 (2001).
- [9] K. Nitsche, & J. Straub, "The critical 'hump' of C<sub>v</sub> under microgravity, results from the D-2 Spacelab experiment 'Wärmekapazität'." *Proc. VI<sup>th</sup> European Symp. on Material Sciences under Microgravity Conditions*. ESA SP-256 (1987).
- [10] A. Onuki, H. Hao, & R.A. Ferrel, "Fast adiabatic equilibration in a single-component fluid near the liquid-vapor critical point." *Phys. Rev. A* **41**: 2256-2259 (1990).
- [11] A. Onuki, & R.A. Ferrel, "Adiabatic heating effect near the gas-liquid critical point." *Physica A* **164**: 245-264 (1990).
- [12] D. Beysens, & Y. Garrabos, "Critical and supercritical fluids and relevant phenomena." In: *Physics and Fluids in Microgravity*. Edited by R. Monti. Taylor & Francis, London and New York (2001).

- [13] A. Onuki, "Phase transition dynamics." Cambridge University Press, Cambridge (2002).
- [14] E.B. Soboleva, "Adiabatic Heating and Convection Caused by a Fixed-Heat-Flux Source in a Near-Critical Fluid." *Phys. Rev. E* **68**: paper 042201 (2003).
- [15] V.I. Polezhaev, A.A. Gorbunov, & E.B. Soboleva, "Unsteady Near-Critical Flows in Microgravity." *Annals of the New York Academy of Sciences* **1027**: 286-302 (2004).
- [16] G. Accary, I. Raspo, P. Bontoux, & B. Zappoli, "Reverse transition to hydrodynamic stability through the Schwarzschild line in a supercritical fluid layer." *Phys. Rev. E* **72**: paper 035301 (2005).
- [17] E.B. Soboleva, "Effect of Energy Sources on Heat Transfer in Near-Critical Fluids." *4th AIAA Theoretical Fluid Mechanics Meeting*. 6 - 9 June 2005. Toronto, Ontario, Canada. AIAA-2005-5379 (2005).
- [18] V.I. Polezhaev, A.A. Gorbunov, S.A. Nikitin, & E.B. Soboleva, "Hydrostatic Compressibility Phenomena: New Opportunities for Critical Research in Microgravity." *Annals of the New York Academy of Sciences* **1077**: 304-327 (2006).
- [19] B.L. Cox, & K. Pruess, "Numerical experiments on convective heat transfer in water-saturated porous media at near-critical conditions." *Transport in Porous Media* **5**: 299-323 (1990).
- [20] V.I. Malkovskii, & A.A. Pek, "Influence of Highly Permeable Fault on Geometry of Thermal Convection of Fluids in the Seafloor Spreading Zones." *Doklady Akademii Nauk* **354**(6): 787 (1997) (in Russian).
- [21] B. Zappoli, R. Cherrier, D. Lasseux, J. Ouazzani, & Y. Garrabos, "Critical slowing down and fading away of the piston effect in porous media." *Condensed Matter - Statistical Mechanics*: eprint arXiv:cond-mat/0601196 (2006).
- [22] D.A. Nield, & A. Bejan, "Convection in Porous Media." Springer-Verlag, New York (1992).
- [23] S.V. Patankar, "Numerical Heat Transfer and Fluid Flow. Computational Methods in Mechanics and Thermal Science." Hemisphere Publ., New York (1980).
- [24] S. Paolucci, "On the Filtering of Sound from the Navier-Stokes Equations." Sandia National Laboratories Report No. SAND 82-8257 (1982).
- [25] L.D. Landau, & E.M. Lifschitz, "Fluid Mechanics, vol. 6." 2<sup>nd</sup> ed. Butterworth-Heinemann, New York (1987).
- [26] R.I. Nigmatulin, "Dynamics of Multiphase media, vol. 1." Taylor & Francis (1990).
- [27] H.E. Stanley, "Introduction to Phase Transition and Critical Phenomena." Oxford University Press, London (1987).
- [28] V.I. Polezhaev, & E.B. Soboleva, "Thermo-Gravitational Convection in a Near-Critical Fluid in a Side-Heated Enclosed Cavity." *Fluid Dynamics* **36**(3): 467-477 (2001).
- [29] V.I. Polezhaev, & E.B. Soboleva, "Unsteady Thermo-Gravitational Convection Effects in a Side-Heated or Cooled Near-Critical Fluid." *Fluid Dynamics* **37**(1): 72-82 (2002).
- [30] A.A. Alexandrov, & B.A. Grigoriev, "The tables of thermophysical properties of water and steam." MPEI Publ. House, Moscow (1999) (in Russian).
- [31] A. Bejan, "On the boundary layer regime in a vertical enclosure filled with a porous media." *Letters in Heat and Mass Transfer* **6**: 93-102 (1979).
- [32] S. Amiroudine, P. Bontoux, P. Larroude, B. Gilly, & B. Zappoli, "Direct numerical simulation of instabilities in a two-dimensional near-critical fluid layer heated from below." *J. Fluid Mech.* **442**: 119-140 (2001).

---

Email address: soboleva@ipmnet.ru (E.B. Soboleva)